

Effectiveness of Nonlinear Optical Loop Mirrors in Dispersion-Managed Fiber Communication Systems Compensated by Chirped Fiber Gratings With Group Delay Ripples

Y. H. C. Kwan, *Member, IEEE, Member, OSA*, K. Nakkeeran, *Member, OSA*,
P. K. A. Wai, *Senior Member, IEEE, Member, OSA*, and P. Tchofo Dinda

Abstract—We examine the effectiveness of using nonlinear optical loop mirrors (NOLMs) to reduce the intersymbol interference in dispersion-managed (DM) fiber communication systems compensated by chirped fiber gratings (CFGs) with group delay ripples (GDR). We show that the use of NOLMs can enhance the transmission performance by more than one order of magnitude in the presence of amplifier noise and random variations in the parameters of the GDR in CFGs. We found that transoceanic transmissions can be achieved when NOLMs are included in the DM optical fiber transmission line compensated by CFGs with GDR whose parameters vary randomly along the transmission line.

Index Terms—Dispersion-managed (DM) systems, gratings, group delay ripples (GDR), nonlinear optical loop mirrors (NOLMs), optical communications.

I. INTRODUCTION

DISPERSION management is a key technique for design and optimization of high-speed long-haul optical fiber transmission systems. Among the existing types of dispersion compensating techniques, the most commonly used lies in dispersion compensating fibers (DCF). In standard terrestrial systems, a DCF with typical dispersion of -90 ps/nm/km and length of ~ 18 – 20 km is used to compensate the cumulated dispersion induced by a 100 km of standard single-mode fiber (SMF). After Ouellette proposed to use chirped fiber gratings (CFGs) for dispersion compensation [1], this device is now well perceived as an attractive dispersion compensating element for future transmission systems. The main virtue of CFGs lies in their compact size. Indeed, to compensate the dispersion induced by 100 km of a standard SMF, we only need ~ 20 cm of CFG; which represents an extremely small fraction

of the length required when using DCF. Chirped fiber grating has many other advantages such as its ability to compensate third-order dispersion [2], its low insertion loss, and negligible nonlinear effects.

It has also been shown that solitons exist in dispersion-managed (DM) fiber transmission systems utilizing ideal CFGs, and operating at speed as much as 100 Gb/s [3], [4]. Experiments have been demonstrated for 10 Gb/s nonreturn-to-zero (NRZ) transmission over 1 000 km [5]. For return-to-zero (RZ) transmission using CFGs, the reported transmission distances are: 2 900 km at 10 Gb/s, 800 km at 4×10 Gb/s, and 500 km at 40 Gb/s [6]–[8].

The major problem that arises when using CFGs for dispersion compensation is the fluctuations of group delay response, known as group delay ripples (GDR), which results from residual multiple reflections induced by various types of imperfections in the grating manufacturing processes [9]. Those imperfections include mechanical vibrations and fluctuations of the power of the ultraviolet (UV) beam used in grating fabrication techniques. The defects in the phase mask can also introduce the GDR. When CFGs are utilized for dispersion compensation in optical transmission line, the GDRs give rise to multiple side peaks (peaks besides the main peak) in the temporal pulse profile. When these side peaks overlap with neighboring pulses, they lead to intersymbol interference (ISI) and degrade the transmission performance. The effects of side peak overlapping are particularly harmful in linear systems because the amplitude of the side peaks increases with the number of CFGs along the propagation distance [10], [11]. Enneser studied the effect of GDR amplitude and GDR ripple period in NRZ systems and found that the system performance is the worst when the ripple period is comparable to the bit rate [12]. The system performance degrades as the ripple amplitude increases.

Meanwhile, it has been shown that solitons exist in grating compensated DM fiber systems with GDR [13], [14]. We have also shown that the use of DM solitons, unlike in linear systems, inhibits the growth of side peaks induced by the GDR in pulse propagation [13]. Although the DM soliton is able to keep the amplitude of the side peaks within relatively small levels, the residual side peaks may still lead to a nonnegligible amount of ISI.

Different methods have been proposed to improve the grating manufacturing processes in order to eliminate the GDR [9], [15]. Komukai *et al.* [9], who pointed out the source of errors in

Manuscript received January 26, 2008; revised June 7, 2008. Current version published January 28, 2009. This work was supported in part by The Hong Kong Polytechnic University under Project No. J-BB9M. The work of K. Nakkeeran was supported by The Royal Society in the form of an International Joint Project Grant.

Y. H. C. Kwan and P. K. A. Wai are with the Photonics Research Centre and Department of Electronic and Information Engineering, The Hong Kong Polytechnic University, Hong Kong (e-mail: canny@eie.polyu.edu.hk).

K. Nakkeeran is with the School of Engineering, King's College, University of Aberdeen, Aberdeen AB24 3UE, U.K.

P. Tchofo Dinda is with the Institut Carnot de Bourgogne (ICB), UMR 5209 CNRS, l'Université de Bourgogne, 21078 Dijon, France.

Digital Object Identifier 10.1109/JLT.2008.928515

the grating manufacturing processes, found that the phase error of the chirped phase mask is the major cause of the GDR in CFGs. They, therefore, proposed a new fabrication method that does not use a chirped phase mask. The method is to start from a uniform fiber Bragg grating and then apply a linear strain gradient in a S-shaped groove using a metal rod to the uniform grating. Since the strain gradient is linear along the grating, it results in a CFG [9]. The resulting CFG has a GDR ripple amplitude as low as 3 ps. Sumetsky *et al.* proposed a new GDR correction method based on an iterative process of UV exposure of the CFG [15]. It was found that this method can reduce the amplitude of the low frequency GDR component from 15 to 2 ps. Apart from the improvement of grating fabrication, Mok *et al.* proposed a 2R regenerator [16], which consists of a dispersion-shifted highly nonlinear fiber, an intense continuous-wave pump and a bandpass filter, to reduce the system penalty caused by the GDR. The optical filter is used to filter out the cascaded sideband generated by the pump and the signal through four-wave-mixing effects. The regenerator however will introduce intensity-dependent timing jitter in the systems.

After the invention of nonlinear optical loop mirrors (NOLMs) [17], it has been shown that conventional soliton can be stabilized by NOLMs in constant dispersion systems [18]. Recently, it has been shown that DM solitons also exist in DM fiber systems using DCFs with NOLMs [19], [20]. Boscolo *et al.* proposed the use of NOLMs in DM fiber systems to obtain autosoliton (highly robust) propagation [21]. This idea was subsequently verified experimentally by Gray *et al.* [20]. Seguinéau *et al.* demonstrated that the transmission performance could be improved by NOLMs in 40 Gb/s DM fiber system with multiple channels [22]. Recently, we have shown that Gaussian-shaped pulse propagation in grating compensated DM fiber systems with NOLMs could achieve transoceanic transmission in the presence of amplifier noise and random variations of ripple period in CFGs along the transmission line [23]. Indeed, the existing grating fabrication processes do not permit to obtain CFGs that have exactly the same GDR parameters. Hence, in a real transmission system, this fact will lead inevitably to random variations of the GDR parameters along the transmission line. Consequently, to obtain a rigorous evaluation of the NOLM action on the GDRs in a real transmission it is necessary to take into account not only random variations in the ripple period but random variations in the other major parameters of the GDR, namely, the ripple amplitude and ripple phase.

In the present paper, we carry out a systematic study of the ability of the NOLMs to enhance the system performance in the DM fiber systems compensated by CFGs. We apply this analysis to the transmission of Gaussian-shaped pulses at a speed of 40 Gb/s over transoceanic distances. To obtain stable DM soliton propagation, an appropriate dispersion map configuration is important. Thus we use the analytical method developed in [24] to minimize the soliton interaction for the new DM soliton grating compensated systems. Using a refined system model that includes random variations in the ripple amplitude, ripple phase, and ripple period, we obtain the dynamical behaviors of pulse propagation in the DM systems compensated by CFGs and assisted by NOLMs. In particular, we show that the

location of the first side peaks (the nearest side peaks besides the central peak), which is related to the GDR period, is the most sensitive parameter that determines the system performance. Furthermore, we found that the NOLMs can substantially increase the interaction length of two neighboring pulses when the separation between the central peak and the first side peak of the neighboring pulses is equal to 1.2 times the pulsewidth. As for the propagation of pulse train is concerned, we have found that in the presence of NOLMs in the system, error-free transoceanic transmissions can be achieved even in presence of random variations in all the GDR parameters.

The paper is organized as follows. The system model is presented in Section II. In Section III-A, we model the GDR as a sinusoidal function and study the random variation of the sinusoidal GDR ripple amplitude, period and phase in grating compensated DM fiber systems without and with NOLMs. In Section III-B, we use the coupled-mode equations to model the grating and vary the grating length, ac coupling constant and chirp constant in gratings and relate the variations of these parameters to that of the GDR parameters. We find that the variations in the grating length and the chirp parameter have significant impact on the system performance. Finally, in Section IV, we draw our conclusion on the effectiveness of NOLMs in DM fiber systems compensated by CFGs with GDR.

II. SYSTEM MODEL

Pulse propagation in an optical fiber system with periodically varying dispersion and Kerr nonlinearity is governed by the nonlinear Schrödinger equation

$$i \frac{\partial q}{\partial z} - \frac{\beta(z)}{2} \frac{\partial^2 q}{\partial t^2} + \gamma |q|^2 q = 0$$

where q is the slowly varying envelope of the electrical field, $\beta(z)$ and γ represent the group velocity dispersion (GVD) and self-phase modulation parameters, respectively. In this paper, all the simulations are carried out for pulsewidths equal or above 5 ps. Hence we neglected the higher-order dispersion and nonlinear effects. The GVD parameter $\beta(z) = \beta$ for $z \neq (n + 1/2)L$, where L is the dispersion map length and n is an integer. The gratings are located at $z = (n + 1/2)L$ and their actions are given by the transfer function $G(\omega)$ such that $\tilde{q}_{\text{out}}(z, \omega) = G(\omega) \tilde{q}_{\text{in}}(z, \omega)$, where ω is the angular frequency, \tilde{q}_{in} and \tilde{q}_{out} are the pulse spectra before and after the gratings, respectively.

In real CFGs, the structure of the GDR is rather complex and depends on the CFG parameters such as the apodization profile, the grating length, etc. These grating parameters have no direct relationship with the GDR parameters. Thus as a simplification, one can assume a sinusoidal model of GDR to study the effect of GDR. We also assume that the grating is lossless and the grating reflectivity bandwidth is much greater than the signal bandwidth [13]. Then the transfer function can be expressed as

$$G(\omega) = \exp \left[i \frac{g}{2} \omega^2 - i \frac{\Gamma}{T_0^2} \cos(\omega T_0 + \theta) + i \frac{\Gamma}{T_0^2} \right]$$

where g is the average lumped dispersion of the grating. The average dispersion of the system is $\bar{\beta} = (\beta L + g)/L$. The parameters Γ , $2\pi/T_0$, and θ are the amplitude, period, and phase of the grating dispersion ripples, respectively. The parameter T_0

is the temporal separation between the side peaks induced by the GDR. The lumped dispersion of the grating is, therefore, given by $g + \Gamma \cos(\omega T_0 + \theta)$.

A more refined model of the grating transfer function $G(\omega)$ is obtained by solving a set of coupled-mode equations [25], which include all the important grating parameters, namely the length of the gratings and the apodization profile. The equations coupling the two propagation modes in the CFGs are given by [25]

$$\frac{dR}{dz} - i \left[\kappa_{dc} + \frac{1}{2} \left(\Delta\beta - \frac{d\phi(z)}{dz} \right) \right] R = i\kappa_{ac}S \quad (1)$$

$$\frac{dS}{dz} + i \left[\kappa_{dc} + \frac{1}{2} \left(\Delta\beta - \frac{d\phi(z)}{dz} \right) \right] S = -i\kappa_{ac}^*R \quad (2)$$

where R and S are, respectively, the forward and backward propagation modes, κ_{dc} is the dc coupling constant which is a function of the average refractive index variation of the grating, and κ_{ac} is the ac coupling constant which is a function of the amplitude of the refractive index variation of the grating. The parameter $\Delta\beta$ is the difference between the propagation constant of the forward- and backward-propagating modes, $\phi(z)$ is the phase change within the grating and the asterisk (*) represents the complex conjugate. In this model, the grating reflectivity bandwidth will be limited and the grating will have a power loss.

III. RANDOM VARIATIONS OF GDR PARAMETERS

In a previous work, it was reported that the transmission performance of a CFG compensated DM fiber system depends strongly on the location of the first side peaks (the nearest neighbor of the central peak), which is inversely proportional to the ripple period [26]. In this respect, two extreme cases have been identified: The first one is the case when the first side peaks of each pulse are located (by either side of the central peak) at the boundary of two adjacent bit slots. In this case, the NOLM action is highly efficient, and can reduce the side peaks by nearly 56 dB. The second extreme case occurs when the first side peak is located exactly at the center of a bit slot. If the given bit slot happens to be occupied by another pulse, then the NOLM action will be less efficient than in the other extreme case. We have also randomly varied the ripple period between these two extreme cases (with a probability of 0.68 to fall within a bit slot), but the amplitude and phase of the GDR were fixed at constant values [23], [26].

Here, we carry out a complete study that gives a deeper insight into the NOLM action in practical situations. We first carry out a basic study of the effect of the separation between a first side peak and a central peak of the neighboring pulse for two-pulse interaction in the DM fiber system. Then, we investigate the individual effect of the variation of other two GDR parameters (ripple amplitude and ripple phase). Next we carry out a complete study, in which we include simultaneous variations of

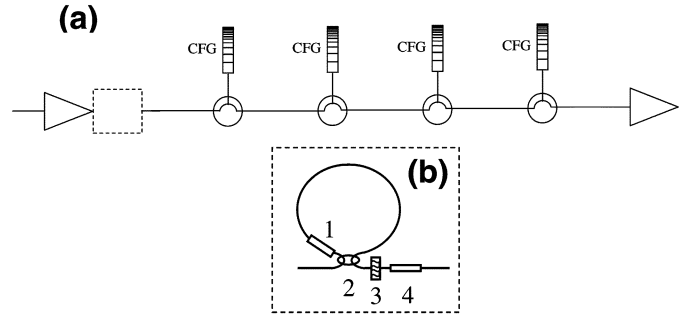


Fig. 1. (a) Schematic of grating compensated DM fiber transmission system and the dashed box is shown in (b) is the configuration of the NOLMs, where 1 and 4: attenuators; 2: 50:50 coupler; 3: filter.

all GDR parameters (ripple amplitude, period and phase) and the amplifier noise, in the system.

We consider a DM fiber system which consists of fiber segments with a CFG located at the middle of the fiber segment and the fiber manufacturer can integrate the CFGs while making the optical fibers. The dispersion map design is important for stable DM soliton propagation and we have developed an analytical method to determine the fiber length and grating dispersion for given pulse and fiber parameters in new DM soliton communication systems [24]. Thus the dispersion map is designed using the analytical method for a map strength of 1.65 to minimize the pulse-to-pulse interactions [24]. The fiber has a dispersion of 1.62 ps/nm/km, nonlinearity of $2 \text{ km}^{-1} \text{ W}^{-1}$, and loss coefficient of 0.2 dB/km. We choose Gaussian input pulses, each having an energy of 0.2 pJ and width of 5 ps, for the simulation of a 40-Gb/s DM fiber system. Using these fiber and pulse parameters in the analytical method [24], we have designed a dispersion map having a fiber segment of ~ 10.25 km long and a grating dispersion of -15.6 ps/nm. The map length ~ 10.25 km is obtained for minimum pulse interaction. In [24], we have shown that if we double the map length but keep the same minimum pulsewidth, we have to approximately double the map strength in the system. As a result the pulse interaction will be increased and the transmission distance will be reduced. Thus the resulting fiber transmission system has an average dispersion of 0.1 ps/nm/km. This dispersion map is used in all cases of our study, except for the two pulses interaction scenario. The amplifier spacing is taken to be four times the dispersion map length, i.e., ~ 41 km. The cumulative ripple effect of four CFGs is large, so it is essential to add NOLM after four CFGs. The schematic of the system is shown in Fig. 1(a). For the system with NOLMs, we place an NOLM after each amplifier. The configuration of the NOLM is shown in the dashed box of Fig. 1(b). The NOLM consists of a 50:50 coupler, a dispersion-shifted fiber with zero dispersion coefficient. In one arm of the NOLM, we use an internal attenuator to break the symmetry. A Gaussian filter with a bandwidth of 110.3 GHz and a loss element (external attenuator) are placed after each NOLM. The filter is used to reshape the pulse to a Gaussian shape and the external attenuator is used to match the input and output pulse powers in the NOLMs. The NOLMs are designed to operate at an input peak power of ~ 1.95 W. The amplifiers in the system with the NOLMs have a gain of 25.2 dB to compensate the total power loss in fibers and NOLMs. We choose different types of

fiber in the loop of NOLMs, the parameters of which are more precisely detailed in Sections III-A and III-B.

A. Modeling GDR by Sinusoidal Function

Since there is no direct relationship between the physical grating parameters and the structure of the GDR in the gratings, here we use a simple sinusoidal function to approximate the GDR structure. We assume that the grating reflectivity bandwidth is much wider than the signal bandwidth, so as to avoid any power loss in the gratings. To investigate the interaction between two pulses, we consider a sinusoidal GDR in CFGs with an amplitude of 5 ps and a period of 0.06 nm. To study the effect of the variation of GDR, we choose the mean value of the ripple amplitude variation to be 3 ps. Komukai *et al.* have demonstrated that the ripple amplitude of a CFG for dispersion compensation could be reduced to 3 ps when the CFG is made by giving a strain to a uniform grating [9]. It has been reported that the ripple amplitude of a CFG for gain flattening could be as low as 1.5 ps, with a dominant period of 0.06 nm [27].

Here we investigate the effect of the first side peaks on the pulse-pulse interactions by launching two Gaussian pulses in the designed system. The fiber has a length of ~ 10.28 km, a dispersion of 1.62 ps/nm/km. Thus the average system dispersion is 0.11 ps/nm/km. The system configuration is shown in Fig. 1. The parameters of NOLMs are the same as that in [23]. We choose the GDR ripple amplitude to be 5 ps. The ripple period is 0.06 nm (7.5 GHz), which leads to a separation between the side peaks of 133.33 ps. We vary the temporal spacing between the two Gaussian pulses and study the interaction length as a function of pulse separation. To perform this study we measure the temporal pulse shift from its original position and the amplitude difference between the two pulses. Unlike the usual two-pulse interaction, here the situation is quite different because of the presence of the side peaks. In usual two-pulse interaction, the temporal separation and the relative phase between them are the only factors which determine the interaction length. Here, an additional and important factor, namely the amplitude jitter, comes into play in the determination of the interaction length. Fig. 2 represents the interaction distance as a function of the separation τ between the two pulses (or equivalently, the separation between the main peaks of the two pulses). As the separation between the first side peak and the central peak is fixed to 133.33 ps for each pulse, we use the variable T to designate the separation between the first side peak of each pulse and the central peak of the other pulse. The interaction process causes each pulse to move away from the center of its rest frame, thereby inducing a modification (increase or decrease) of the separation between the two pulses. The interaction also causes amplitude variations in the pulse profile. We define the *interaction distance* as the minimum between the two following characteristic distances: The first one is the propagation distance at which the pulse displacement from its original position becomes greater than the initial FWHM $W_0 = 5$ ps. The second one is the distance at which the amplitude difference between the two pulses becomes greater than $\sim 0.3\%$ of the initial pulse amplitude. One can clearly observe two main regions in the interaction distances:

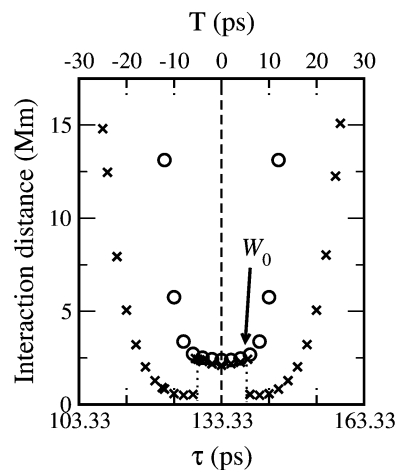


Fig. 2. The interaction distance as a function of separation between the pulses in system without (crosses) and with (circles) NOLMs. The side peaks separation from the main peak is 133.33 ps and the x axis at the top shows the separation between the first side peak of a pulse and the central peak of its neighboring pulse. The vertical dashed line marks where the first side peak is exactly located at the central peak of neighboring pulse.

(i) The first one corresponds to $|T| \leq W_0$, in which the first side peaks strongly overlaps with the central peak of neighboring pulse ($T = 0$ corresponds to the extreme case where the location of the first side peak coincide exactly with that of the central peak of neighboring pulse). In this region, the interaction distance without (crosses) and with (circles) NOLMs are essentially identical. Here, the NOLM action cannot selectively suppress the first side peak without causing a strong alteration of the central peak of neighboring pulse. Thus amplitude fluctuation will occur and it depends on the phase difference as shown in [28]. In this region, the interaction distance is determined by the amplitude jitter.

(ii) The second outstanding region corresponds to $|T| > W_0$, in which the first side peak weakly overlaps with the central peak of neighboring pulse. In this case, the system with NOLMs yields a larger interaction distance, which increase strongly as $|T|$ increases (i.e., as the overlapping between the first side peak and the central peak of neighboring pulse vanishes). Thus, it is clear from Fig. 2 that NOLMs can efficiently suppress the first side peak only when they are sufficiently far away from the central peak of neighboring pulse. Pulse temporal position may shift when the peak power of the pulses are not the same. Thus timing jitter may occur in the presence of side peaks as mentioned in [28]. Here the timing jitter is dominant in the interaction process. This is the reason for the presence of discontinuities (at $T = W_0$) in the data points (crosses) in Fig. 2. Note that W_0 is the initial FWHM.

We will show in following sections that this simple analysis of the two-pulse interaction is helpful to understand the dynamical behavior of a pulse train propagation with fixed pulse separation and varying side peaks location due to the variation of the ripple period along a transmission line.

1) *Random Variations of Ripple Period:* Recently we have studied a system with random variation in the GDR ripple period of the CFGs along the transmission line [23], [26]. In [26], we found that the value of ripple period is the dominant factor in the

system performance. If we choose the ripple period such that the location of first side peaks is at the boundary of bit slot, then the system results in transoceanic transmission. However, if the location is at the centre of bit slot, then the transmission distance is significantly reduced [26]. In practice, it is difficult to make two identical gratings, we, therefore, considered the random variation in the ripple period of the CFGs in [23]. We choose the variation such that the location of the side peaks is varied within one bit slot in 68% chance to show the impact of side peaks. In [23], the mean of ripple period variation is 0.06 nm (7.5 GHz) and the standard deviation is 0.0056 nm (0.7 GHz). Here we examine the effects of variations of the ripple period in a Gaussian distribution fashion with a mean of 0.064 nm (8 GHz) and standard deviation of 0.0028 nm (0.35 GHz) in the DM fiber system compensated by CFGs. In this case, a bit rate of 40 Gb/s will create a situation that the first side peaks strongly overlap with the central peak of neighboring pulses. For a distance of 10 000 km, the transmission line contains 976 CFGs in total, which can give a pretty good Gaussian distribution in the variations of the GDR parameters.

We launch a 128-bit Gaussian-shaped bit sequence with a mark ratio of 0.5 and bit window of 25 ps (40 Gb/s speed of transmission) in the system without and with NOLMs. The pulse energy is taken to be 0.2 pJ with a pulsewidth of 5 ps. For the NOLMs, the loop length is 1.08 km, the nonlinearity parameter is $4 \text{ km}^{-1}\text{W}^{-1}$, and the loss coefficient is 0.3 dB/km. The lumped loss of the in-loop attenuator is 12.1 dB and the loss element placed after the filter is 0.06 dB [see Fig. 1(b)]. In this study, we investigate the system performances for two different mean ripple periods, 0.06 nm (7.5 GHz) [27] and 0.064 nm (8 GHz) [10]. We randomly vary the ripple period of the CFGs along the transmission line in a Gaussian distribution fashion having a standard deviation of 0.0028 nm (0.35 GHz). Thus for these two situations, we vary the ripple period in the range 7.15–7.85 GHz around the mean value of 7.5 GHz, and in the range 7.65–8.35 GHz around the mean period of 8 GHz. This leads to a variation of the separation between the first side peak and the central peak, from 127 ps to 140 ps for the mean period of 7.5 GHz, as illustrated in Fig. 3(a), and from 120 ps to 131 ps for the mean period of 8 GHz, as illustrated in Fig. 3(b).

Fig. 3(a) corresponds to a situation where the variation in the location of the first side peak spreads over a region that overlaps two consecutive bit slots. This region includes one half of the first bit and a small portion of the next one. This situation corresponds to a configuration of relatively weak overlapping between the first side peak and the central peak of neighboring pulse, in which one may expect the NOLM action to effectively suppress the first side peak. Fig. 3(b) corresponds to a situation where the variation in the location of the first side peak spreads over a region that is situated entirely in one bit slot. This situation corresponds to a configuration of relatively strong overlapping between the first side peak and the central peak of neighboring pulse, in which one may expect the NOLM action to only mildly suppress the first side peak, as we showed in the above analysis of the two-pulse interaction. If we transmit a pulse train made of logical “1” in all the bit slots, one could expect there to be insignificant improvement of the quality of the transmission when using NOLMs. Now, in transmission of a pseudo-

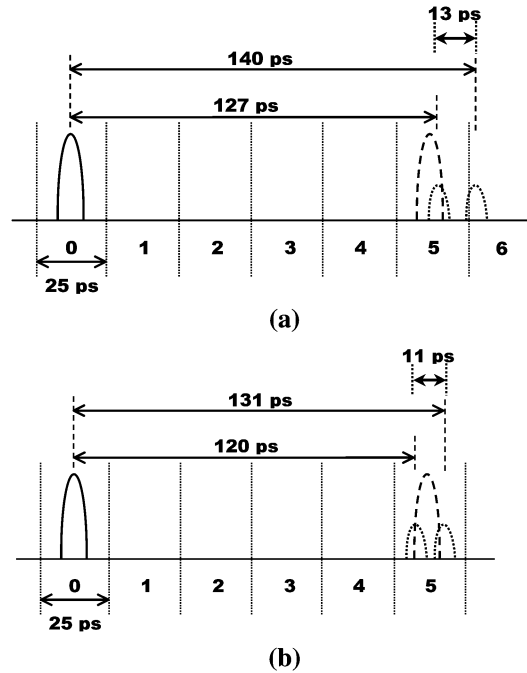


Fig. 3. Illustrations of the locations of the proximity central peak and the first side peak for a ripple period of (a) 7.5 GHz and (b) 8 GHz, respectively.

random bit sequence (PRBS), nearly half of the bit slots are empty (logical “0”), and there each first side peak have 50% chance to be placed in an empty bit slot. In other words, in case of a PRBS transmission in the situation corresponding to Fig. 3(b), nearly half of all first side peak, which will inevitably take place within the empty bit slots, will be well isolated from the central peak of neighboring pulse and can be efficiently suppressed by the NOLM action. Thus, the situation in Fig. 3(b) may turn out to be not that much unfavorable when compared with the case in Fig. 3(a). To clarify this point, we have carried out numerical simulation of PRBS transmission in the system, in which the GDR ripple amplitude and phase are kept constant to 3 ps and π , respectively. To evaluate the transmission performances, we use a standard approach, in which one assumes Gaussian probability density functions for the input voltage to the decision circuit for both the “0” and “1” levels. Then one evaluates the Q -factor from the mean values μ_0 and μ_1 , and the standard deviations σ_0 and σ_1 of the “0” and “1” levels, respectively. These mean values and standard deviations are obtained by the peak voltage within the bit slot. The amplitude Q -factor, which serves as a measure of the amplitude jitter, is defined by $Q_A \equiv (\mu_1 - \mu_0)/(\sigma_1 + \sigma_0)$, whereas the timing Q -factor serves as a measure of the timing jitter and is defined by $Q_T \equiv 0.7T_d/\sigma_T$, where $T_d = 25 \text{ ps}$ is the size of the bit slot, and σ_T is the standard deviation of the “1” with respect to the center of the bit slot and is obtained by the temporal position of the peak voltage. Here, the transmission distance is defined as the maximum distance over which the smaller of the two Q -factors, $\min(Q_A, Q_T)$, remains higher than 6. Note that the Q -factor is given in linear units and the value $Q = 6$ corresponds to a bit-error ratio of 10^{-9} [29], [30].

Fig. 4 shows the Q -factors of the transmission performance without (dashed) and with (solid) NOLMs in the system for the

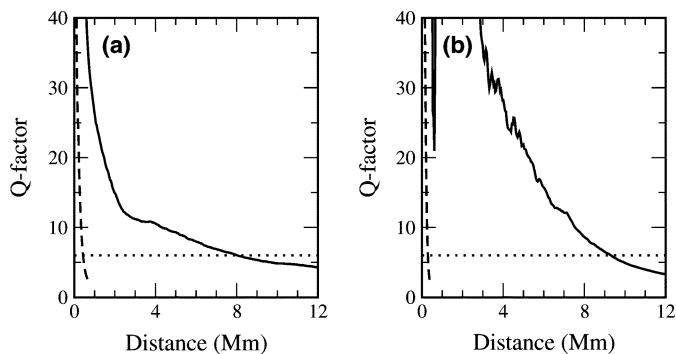


Fig. 4. The Q -factors in the system without (dashed curve) and with (solid curve) NOLMs. The ripple period is randomly varied in the CFGs along the transmission line in a Gaussian distribution fashion with mean values of (a) 7.5 GHz and (b) 8 GHz and standard deviation of 0.35 GHz. The ripple amplitude and phase are kept constant at 3 ps and π , respectively.

mean ripple period of (a) 7.5 GHz and (b) 8 GHz. The dotted horizontal line represents $Q = 6$. In Fig. 4(a), the error-free transmission distances without and with NOLMs are 0.41 and 8 Mm, respectively. In Fig. 4(b), the transmission distances are, respectively, 0.29 and 9.3 Mm for the system without and with NOLMs. We attribute the surprisingly good transmission performance in the case of Fig. 4(b), to the fact that nearly 50% first side peaks that fall within empty bit slots, and are thus well isolated from neighboring central peaks. In addition, the variations in the ripple period reduce the possibility of the first side peaks to be exactly located on the central peak of neighboring pulse.

The NOLM acts as a nonlinear intensity filter which causes the pulse peak power to remain trapped around a well specified value, while the parts of the pulse profile which are much smaller than the peak power are strongly attenuated when passing through the NOLM; hence the suppression of the pedestals containing the side peaks.

The second outstanding result in Fig. 4 is that the DM fiber system can achieve transoceanic transmission even with random variations of the ripple period in CFGs along the transmission line.

2) *Random Variations of Ripple Amplitude:* Now, we study the variations of the ripple amplitude in CFGs along the transmission line. The DM fiber system and NOLM parameters remain the same as in the case of random variations of the ripple period, considered above. We also launch a 128-bit pulse sequence into the system. In this investigation, the ripple period and the ripple phase are kept constant. The ripple phase is chosen to be π . We study the effect of variations in the ripple amplitude for two different ripple periods, those are 0.06 nm (7.5 GHz) [27] and 0.064 nm (8 GHz) [10], respectively. The separation T is 8.33 ps for the ripple period of 0.06 nm (7.5 GHz), and zero for the ripple period of 0.064 nm (8 GHz). We randomly vary the ripple amplitude of the CFGs in a Gaussian distribution fashion along the transmission line. The distribution has a mean value of 3 ps (that is same as the value reported in [9]) and standard deviation of 0.5 ps. Since the ripple amplitude could be as low as 1.5 ps [27], we set the lower bound of the random variation of the ripple

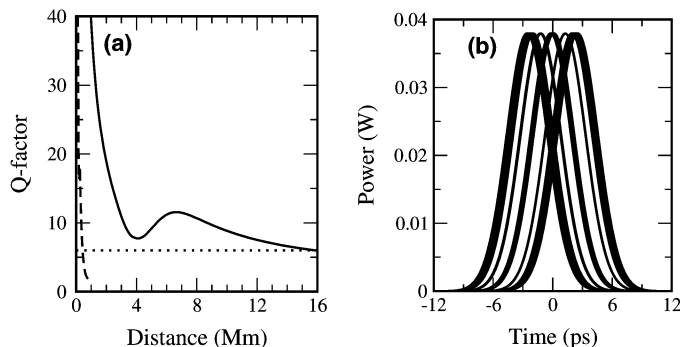


Fig. 5. (a) The Q -factors in the system without (dashed curve) and with (solid curve) NOLMs. (b) The corresponding eye diagram in the system with NOLMs at 15.8 Mm. The ripple amplitude is randomly varied in the CFGs along the transmission line in a Gaussian distribution fashion with a mean value of 3 ps and standard deviation of 0.5 ps. The ripple period and phase are kept constant at 7.5 GHz and π , respectively.

amplitude to be 2 ps. We have also fixed the upper bound of the ripple amplitude to 4 ps. Fig. 5(a) shows the Q -factors of the transmission performance without (dashed) and with (solid) NOLMs in the system having the ripple period of 7.5 GHz in the CFGs. The eye diagram at 15.8 Mm is shown in Fig. 5(b) for system with NOLMs. The transmission distance in the system with NOLMs is one order of magnitude longer than that without NOLMs. The use of NOLM significantly enhances the system performance. The transmission distance in system with NOLMs (15.8 Mm) is nearly twice when compared with the results reported in Fig. 4(a), 8 Mm. It clearly shows that the ripple amplitude variation (33%) is less harmful for the system performance than the ripple period variation (5%), which is an important result of the present work.

On the other hand, for the ripple period of 8 GHz, the error-free transmission distance is 0.25 and 0.7 Mm for the system without and with NOLMs, respectively. In this case, the first side peaks location (125 ps) is exactly an integral multiple of the bit slot (25 ps). This causes the first side peaks to remain exactly overlap with the central peak of neighboring pulse throughout the propagation distance, in nearly half of the bit slots. In this worst case scenario such first side peaks cannot be suppressed by the NOLMs. Hence, the system suffers large intensity jitter that is caused by the energy exchange between the first side peaks and its central peak.

From the simulation results, it is obvious that the NOLMs are very effective to reduce the effect of GDR even with variations in the ripple amplitude in the grating-compensated DM soliton system if the first side peak does not locate exactly at the center of a bit-slot.

3) *Random Variations of Ripple Phase:* Here, we vary the ripple phase in CFGs along the transmission line for a fixed ripple amplitude of 3 ps and period of 7.5 GHz. Ripple phase is the relative phase between the center frequency of the pulse spectrum and the GDR. Figs. 6(a) and (b) show the ripple phase of 0 and π , respectively. Solid and dashed curves represent dispersion ripples of a CFG and the pulse spectrum in the system. The other system parameters including the input bit sequence remain the same as in previous simulations. The ripple phase of the CFGs is randomly varied along the transmission distance in

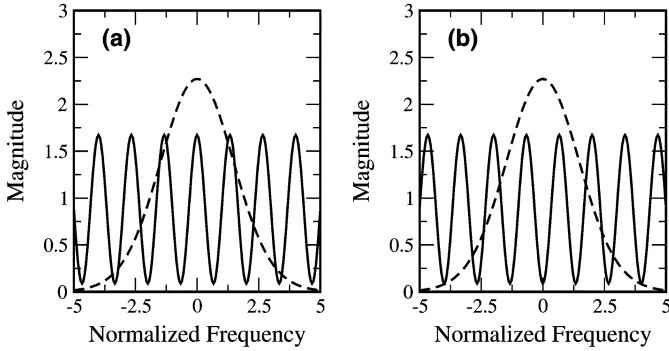


Fig. 6. Example of ripple phase of (a) 0 and (b) π , respectively. Solid curve shows the dispersion ripples of a CFG and dashed curve shows the pulse spectrum.

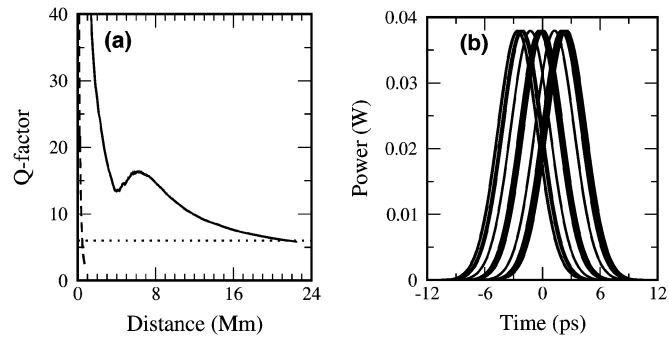


Fig. 7. (a) The Q -factors in the system without (dashed curve) and with (solid curve) NOLMs. (b) The corresponding eye diagram in the system with NOLMs at 21.6 Mm. The ripple phase is randomly varied in the CFGs along the transmission line in a Gaussian distribution fashion with a mean value of π and standard deviation of 0.25π . The ripple amplitude and period are kept constant at 3 ps and 7.5 GHz, respectively.

a Gaussian distribution fashion with a mean value of π and a standard deviation of 0.25π .

Fig. 7(a) shows the Q -factors along the pulse propagation in the system without (dashed) and with (solid) NOLMs. The error-free transmission distances are, respectively, 0.45 and 21.6 Mm in the system without and with NOLMs. The action of NOLMs can increase the transmission distance by 43 times when compared with the system without NOLMs. The eye diagram in the system with NOLMs at 21.6 Mm is shown in Fig. 7(b). To study the effect of the ripple phase, we obtain the DM soliton solution in the system with different values of a fixed ripple phase. We found that the relative phase between the central peak and the side peaks of the DM soliton solution depends on the ripple phase. Fig. 8 shows the relative phase between the central peak and the first side peaks for different values of ripple phase in the system. The crosses and circles represent the data points of the phase difference for the left and right first side peak, respectively. The variations in the ripple phase of the CFGs vary from one grating to the other may lead to drastic changes on the amplitude of the side peaks between the limits of perfect cancellation (due to opposite phase difference) and sustained growth [13] (due to same phase difference). Therefore, the variation of the ripple phase of the CFGs along the transmission line could enhance the system performance due to the reduction of the side peaks growth. It is however, not

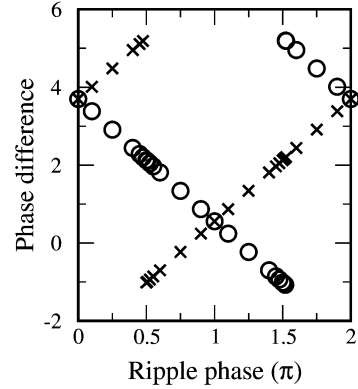


Fig. 8. The relative phase between the first side peaks and the central peak of the stable pulse for different ripple phase in the grating compensated DM fiber system with NOLMs. The crosses and circles are the data points for the left and right first side peaks, respectively.

the case when the ripple period is 8 GHz, where we found that the transmission distance (0.2 Mm) is the same for the system without and with NOLMs. When the side peaks separation is an integral multiple of the bit slot, the phase cancellation or addition occur between the side peaks and the central peak of other pulses which decreases or increases the peak power of the central peak of the pulses in the system. The addition of the NOLMs cannot compensate for these changes. If the increased peak power is much greater than the stable operation power of the NOLMs, it is possible that the pulse could be switched-off by the NOLMs.

The variation of ripple phase in general can enhance the system performance with the action of the NOLMs, except for the case when the bit rate is an integral multiple of the ripple period.

4) *Random Variations of GDR Parameters With Amplifier Noise:* In the previous subsections we have discussed the individual effect of each GDR parameter on the system performance. Here, we include the simultaneous variation of all GDR parameters (ripple amplitude, period, and phase) in the same system studied earlier. In fact, this simulation is closer to the practical situation, where all the ripple parameters may randomly vary along the transmission line. We independently choose the variations of all the ripple parameters to follow a Gaussian distribution. In other words, the variations of a given parameter has no relationship to the other two parameters. The parameters of the Gaussian distribution, namely the mean value, standard deviation, upper bound and lower bound remains the same as previous sections. The system performance for the mean ripple period of 7.5 GHz is shown in Fig. 9(a) and for the mean ripple period of 8 GHz is shown in Fig. 9(b). The dashed and solid curves represent the Q -factors of the system without and with NOLMs, respectively. The transmission distances in the system with a mean ripple period of 7.5 and 8 GHz are nearly the same and, respectively, 9.1 and 8.5 Mm. The transmission distance is significantly increased even in the case of mean ripple period 8 GHz, because of the random variation of the ripple period.

To study the accumulated effect of higher order dispersion on the huge propagation distance, we include the effect of third-

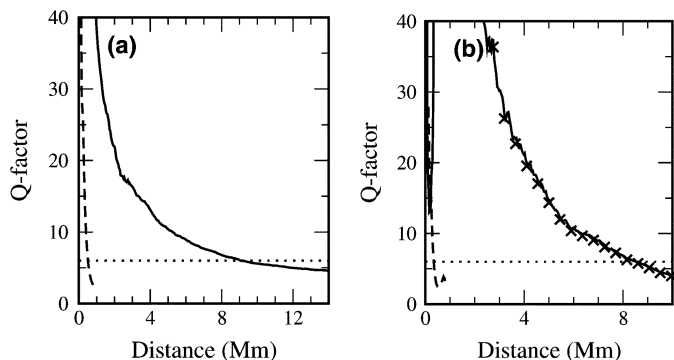


Fig. 9. The Q -factors in the system without (dashed curve) and with (solid curve) NOLMs. The ripple amplitude, period and phase are randomly varied in the CFGs along the transmission distance. The mean ripple period is (a) 7.5 GHz and (b) 8 GHz. The mean and standard deviation are same as in Figs. 4, 5, and 7. The crosses in (b) represent the results when the effect of third-order dispersion are included. The third-order dispersion coefficients for the fibers and CFGs are $0.1 \text{ ps}^3/\text{km}$ and -1.025 ps^3 , respectively. The system has no amplifier noise.

order dispersion in the optical fibers and the CFGs. The respective third-order dispersion coefficients for the fibers and CFGs are $0.1 \text{ ps}^3/\text{km}$ and -1.025 ps^3 . The third-order dispersion of the CFG is chosen to compensate the cumulated third-order dispersion effect of the optical fiber in a dispersion map. We choose the case in which the mean ripple period is 8 GHz. Fig. 9(b) shows the system performance. The results are represented by crosses and the error-free transmission distance is 8.4 Mm. The results show that the effect of third-order dispersion on the system performance is negligible even with random variation in the CFGs. We, therefore, neglect the effect of higher order dispersion in the rest of the discussion.

Next, we include the effect of amplifier noise in the simulation. The noise figure is considered to be 4.5 dB in each amplifier. In this case, we only consider the mean ripple period of 7.5 GHz since the transmission performance is similar for both mean ripple periods (7.5 and 8 GHz). Fig. 10 illustrates the Q -factors of the transmission performance without (dashed) and with (solid) NOLMs in the system. The Q -factors are calculated using 50 realizations in PRBS under the influence of the amplifier noise. The error-free transmission distances without and with NOLMs are 0.49 and 8.6 Mm, respectively. Fig. 10(b) shows the corresponding eye diagram of a pulse sequence at 8.6 Mm. It follows from this figure that the NOLMs can effectively stabilize the pulse peak power even in the presence of amplifier noise [18].

The results show that the use of NOLMs can substantially reduce the amplitude of side peaks and the amplifier noise simultaneously in the grating-compensated DM fiber system having random variations of ripple amplitude, period, and phase in the CFGs along the transmission distance.

B. Modeling of CFG by Coupled-Mode Equations

In grating fabrication, the three major grating parameters; grating length, ac coupling constant and the chirp constant, may vary. Variations in the grating length are due to [9]: (i) Mechanical vibrations in the equipment during grating fabrication. (ii) The misalignment in the spacing between the phase mask and the fiber. (iii) Thermal expansion in the transmission line

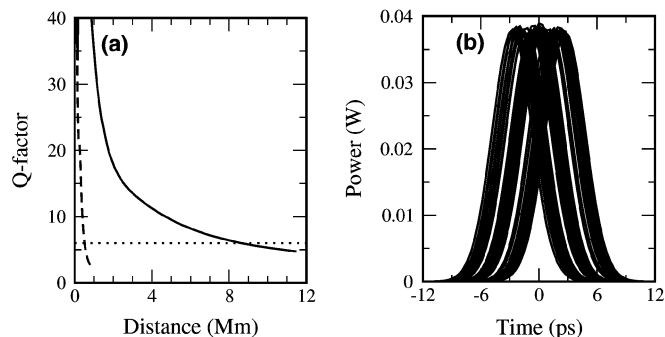


Fig. 10. (a) The Q -factors in the system without (dashed curve) and with (solid curve) NOLMs. (b) The corresponding eye diagram in the system with NOLMs at 8.6 Mm. The ripple amplitude, period and phase are randomly varied in the CFGs along the transmission distance and the mean ripple period is 7.5 GHz. The mean and standard deviation are same as in Fig. 9. The system has amplifier noise.

due to daily change in temperature. (iv) Deviation in the manufacturing methods using pressure, bending, strain, or temperature change in the processes.

The variations in the ac coupling constant could be caused by (i) The power and mode fluctuation in the UV beam which is used to fabricate the CFGs. (ii) The refractive index fluctuation due to the temperature and stress in the use of gratings. (iii) The fluctuation in the fiber core, which leads to changes in refractive index. (iv) The variation of concentration in the hydrogen-loaded fiber used to increase the photosensitivity.

The fluctuation of the chirp constant F could be caused by: (i) the imperfection in the phase mask, like the pitch fluctuations and the variations in the depth of the groove in the phase mask; (ii) mechanical vibration in scanning the UV light; (iii) deviation in some manufacturing processes to duplicate gratings: bending or pulling the fiber.

Ania-Castañón *et al.* [14] have studied the tolerance of grating compensated DM soliton systems with respect to random variations in the grating parameters. In [14], the gratings are modelled by coupled-mode equations [25], in which the three major physical parameters of the CFG (grating length, ac coupling constant and the chirp constant) are uniformly varied. Here, we include the NOLMs in the system. We also vary the three grating parameters, and we study the effectiveness of using the NOLMs action in such systems. As there is no direct relationship between the grating parameters in the coupled-mode equations and the GDR parameters, we first investigate the changes of the GDR parameters for different grating parameters.

We launch a 128-bit Gaussian-shaped PRBS with mark ratio of 0.5 and bit window of 25 ps in the system without and with NOLMs. The pulse energy is taken to be 0.2 pJ and the width is 5 ps, for a transmission speed of 40 Gb/s. The dispersion map parameters are the same as in previous sections. In practical implementation, we shorten the loop length of NOLMs to be 0.21 km by using a highly nonlinear fiber [22]. The fiber has a zero dispersion coefficient, a nonlinearity coefficient of $20 \text{ km}^{-1}\text{W}^{-1}$, and loss coefficient of 0.55 dB/km. The loss of the in-loop attenuator is 12.3 dB and the loss element placed after the filter is 0.08 dB. In the coupled-mode equations, the

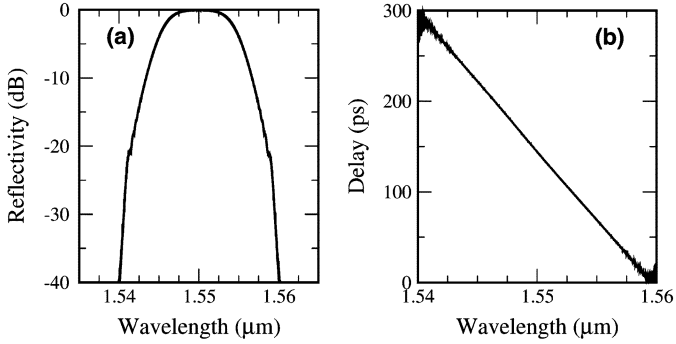


Fig. 11. (a) Reflectivity and (b) group delay spectrum of the grating that modeled by the coupled-mode equations. The grating length is 3 cm and $\kappa_{ac} = 1.75 \text{ mm}^{-1}$ with Gaussian apodization profile.

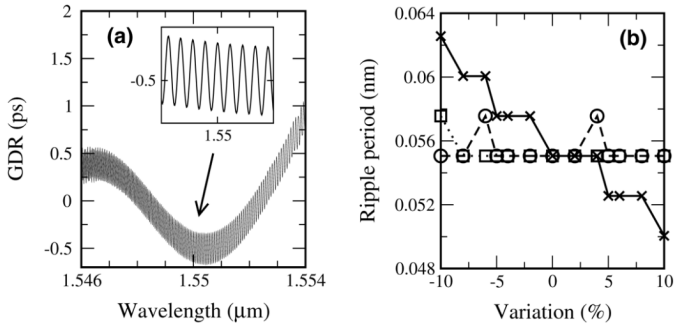


Fig. 12. (a) The GDR spectrum of the grating that is obtained from the coupled-mode equations and fitting the delay spectrum with a straight line as shown in Fig. 11. (b) The ripple period versus the change of grating parameters: grating length L_g (crosses), coupling constant κ_0 (circles), and the chirp constant F (squares).

CFG has a length of 3 cm and the power loss at the center of the grating reflectivity is 0.084 dB. Thus the gain in each amplifier used here is 25.5 dB, which is slightly greater than that in previous simulations because of the power loss in the four gratings in an amplifier spacing. We adopt a Gaussian apodization profile [1], and take the amplitude of the refractive index variation along the grating to be of the following form:

$$\kappa_{ac}(z) = \kappa_0 \exp \left[\frac{-2(z - 0.5L_g)^2}{L_g^2} \right]$$

where κ_0 is the amplitude of the index fluctuation and L_g is the grating length. We choose the maximum index fluctuation κ_0 to be 1.75 mm^{-1} and the dc coupling constant $\kappa_{dc} = 0$ in Eqs. (1) and (2). The phase change ($d\phi/dz$) is equal to $F(z - 0.5L_g)/L_g^2$ and the chirp constant $F = 4341.8$. The grating reflectivity and delay spectrum are shown in Figs. 11(a) and (b), respectively. The average grating dispersion is -15.56 ps/nm . Using curve fitting in group delay, we obtain the GDR in the grating profile as shown in Fig. 12(a). The inset is the zoom-in at the center Bragg wavelength. At the center of the grating reflectivity or at Bragg wavelength, the ripple amplitude is $\sim 0.16 \text{ ps}$, the ripple phase is 0 and the ripple period is 0.055 nm (6.88 GHz). The locations of the left and right first side peaks of the stable pulse in the system are slightly different because of the asymmetric structure of the

group delay ripple spectrum. The separations between the central peak and the left and right first side peaks are $\sim 145 \text{ ps}$. The ripple amplitude is relatively small because of the nature of the apodization profile, which is close to zero at both ends of the gratings. This can smooth the delay fluctuation, and one can neglect the experimental errors in grating manufacturing processes. In the absence of variations of grating parameters and noises, the transmission distance for a 128-bit PRBS is 3.4 Mm and over 20 Mm, in the system without and with NOLMs, respectively. We have also studied the system using a sinusoidal GDR modeling with the same values of GDR parameters as for the coupled-mode equations (ripple amplitude = 0.16 ps, period = 0.055 nm and phase = 0). Although the ripple amplitude is low, we found that the error-free transmission distance without NOLMs is 1.5 Mm which is nearly half the transmission distance obtained by use of the coupled-mode equations. The error-free transmission distance is over 20 Mm with NOLMs. It shows that the sinusoidal GDR model overestimates the effect of GDR. Despite the overestimation, the sinusoidal function is very useful in the understanding of the effect of GDR parameters on transmission performance. Since a change in one grating parameter can affect several GDR parameters, its effect is more complex.

Understanding the relation between the grating parameters and the ripple parameters is important to alleviate the effect of GDR. In the following, we take the Bragg wavelength as a reference point to characterize the GDR with respect to the variations in the values of L_g , κ_0 and F . As the grating length L_g increases from -10% to 10% , we found that the ripple amplitude increases linearly, the ripple period decreases linearly, the ripple phase decreases and the reflectivity increases. Note that the magnitude of the average dispersion of the grating increases quadratically as the length L_g increases [1]. For instance, the dispersion value is increased by 21% when the grating length L_g is increased only by 10%. For the coupling constant κ_0 we found that as κ_0 increases, the ripple amplitude increases linearly, the ripple phase reduces linearly and the grating reflectivity increases. It is worth noting that the ripple period is unchanged when κ_0 varies from -10% to 10% . Also, the magnitude of the average dispersion is increased by only 0.7%, as κ_0 is increased by 10%. As for the variation of F , the ripple phase oscillates and ripple period remains almost constant. The ripple amplitude decreases linearly as the chirp constant (also known as phase change constant) F increases. Note that the change in the average grating dispersion is inversely proportional to the chirp constant [1]. Thus the average-dispersion magnitude is decreased by 8.8%, as the chirp constant is increased by 10%. The evolution of the ripple period as a function of the different grating parameters is illustrated in Fig. 12(b). The x -axis corresponds to the variation of the grating parameters in percentage. The crosses, circles and squares are the data points representing the grating length L_g , the coupling constant κ_0 and the chirp constant F . In Fig. 12(b), the variation of the ripple period with respect to κ_0 and F are almost the same (close to the numerical wavelength step size of 0.0025 nm). Thus the ripple period remains constant irrespective of the variations in κ_0 or F . From Fig. 12(b), the grating length L_g would be the dominant parameter that affects the system performance as it can change the

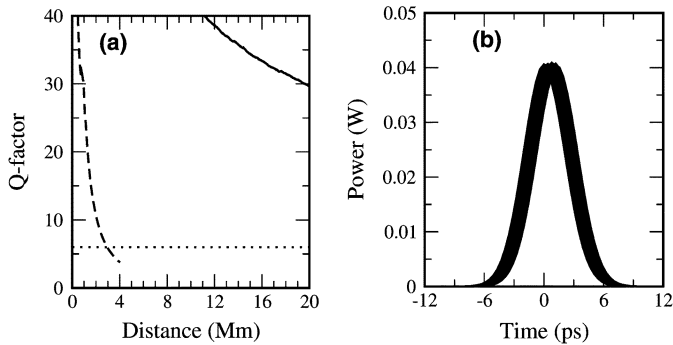


Fig. 13. (a) The Q -factors in the system without (dashed curve) and with (solid curve) NOLMs. (b) The corresponding eye diagram in the system with NOLMs at 20 Mm. The grating is modeled by the coupled-mode equations and the grating length, coupling constant and chirp constant are randomly varied in the CFGs along the transmission distance. The system has amplifier noise.

ripple period. The grating length also significantly affects the value of the average dispersion of the grating when compared to other grating parameters (κ_0 and F).

Now, we vary the grating parameters individually in a normal distribution fashion, and we launch a 128-bit sequence in the system. For a standard deviation of 3% of the mean value of the respective varying parameter, we found that the system can achieve transmission distance over 10 Mm in all the three cases. When the standard deviation is 4% of the mean value, the system with variation of grating length L_g can execute error-free transmission over only 6.8 Mm. However, the system with variation of κ_0 or F can still achieve transmissions over 20 Mm. When the standard deviation is increased to 5% of its mean value, the system can no longer achieve transoceanic distance in the presence of variations of the grating length L_g or chirp constant F because of the large variation in the magnitude of the average dispersion. Thus, which in turn significantly affect the average dispersion of the system. In the presence of variations in the coupling constant κ_0 with a standard deviation of 5%, the transmission distance can still go up to 20 Mm. This shows that variations in the coupling constant has smaller impact on the system performance when compared with the effects of variations in the grating length or chirp constant.

Next, we vary all the grating parameters simultaneously and reduce the standard deviation with respect to the mean value to 0.8% in κ_0 and F , and 0.6% in the grating length. There is 95% chance for the deviations of the grating parameters from their mean values to lie within twice of their standard deviations. For example, the grating length L_g fluctuates within 1.2% and chirp constant F or coupling constant κ_0 varies within 1.6% of their mean values with a 95% probability. We launch the PRBS into the system and obtain an error-free transmission distance over 20 Mm. These variations are quite similar to those reported in [14]. They used a uniform distribution within 1% of the grating parameters for the formation of the soliton.

We also include the amplifier noise with a noise figure of 4.5 dB to model the real situation and use 50 sets of random sequence to simulate the noise and PRBS. The grating parameters L_g , κ_0 and F are varied in a Gaussian distribution and have mean values of 3 cm, 1.75 mm^{-1} , 4341.8 and standard deviations of 0.018 cm, 0.014 mm^{-1} , 34.7, respectively. In the

scanning method to fabricate the CFG, the accuracy of writing the grating length can be up to $2 \mu\text{m}$, however the grating length fluctuations may be larger in other grating manufacturing methods. Thus the chosen variations are already larger than the best gratings technology can offer today. Practically, the grating dispersion value can vary with a fluctuation of 1.7%, which can be obtained by changing L_g by 0.8% or κ_0 by 1.7% in the coupled-mode Fig. 13(a) shows the average Q -factors obtained in the system without (dashed) and with (solid) NOLMs along the propagation distance, respectively. The error-free transmission is over 20 Mm for the system with NOLMs. The eye diagram for the system with NOLMs at 20 Mm is shown in Fig. 13(b). This result demonstrates the efficiency of the NOLMs to enhance the system performance even in the presence of amplifier noise and variations in the physical grating parameters.

IV. DISCUSSION AND CONCLUSION

In this paper, we have clearly demonstrated the use of NOLMs is very effective to improve the system performance in grating compensated DM fiber systems with GDR. It is important to notice that the NOLMs stabilize the pulse peak power at a stable operation point and suppress the pedestals of the pulse profile, thus eliminating the growth of the side peaks caused by the GDR. Depending on the value of the ripple period, the location of the side peaks may strongly or weakly interact with the central peak of the neighboring pulses. In the strong interaction case, the NOLMs cannot selectively suppress the side peaks. In the systems with amplifiers, the pulse peak power fluctuates because of the amplifier noise and the interaction between the side peaks and the central peak of the other pulses. In this case, the system is more prone to deviate away from the stable operating condition for the NOLM.

We have studied the effect of the random variations of the GDR ripple amplitude, ripple period and ripple phase in CFGs along the transmission lines. By randomly varying the ripple amplitude, period and phase, in a Gaussian distribution fashion with mean values of 3 ps, 7.5 GHz, and π , and standard deviations of 0.5 ps, 0.35 GHz, and 0.25π , respectively, we have found that the system performance with the NOLM action can reach transoceanic distances, even in the presence of variations of all GDR parameters along the propagation distance. We have found that the ripple period is the dominant parameter which affects the system performance.

We have also studied the relationship between the physical grating parameters and the GDR parameters and investigated the tolerance of the system performance with respect to variations in the grating parameters. The GDR ripple period was found to be highly sensitive to variations in the grating length. Other physical parameters like chirp constant, which are related to the average grating dispersion, can also induce degradations in the system performance. We find that in the presence of amplifier noise and slight random variations in all grating physical parameters, the transmission distance can still reach transoceanic distances in systems with NOLMs.

In conclusion, we have shown that the use of NOLMs can substantially improve the transmission performance in the grating-compensated DM fiber systems with GDR in CFGs. We have

shown that the use of NOLMs permits error-free transoceanic transmission of Gaussian-shaped pulses in the presence of amplifier noise and random variations of the GDR parameters in CFGs along the propagation distance. It shows that the proposed method can be very effective to improve the transmission performance of future high-speed long-distance transmission systems.

ACKNOWLEDGMENT

P. Tchofo Dinda acknowledges The Hong Kong Polytechnic University for their hospitality.

REFERENCES

- [1] F. Ouellette, "Dispersion cancellation using linearly chirped Bragg grating filters in optical waveguides," *Opt. Lett.*, vol. 12, no. 10, pp. 847–849, Oct. 1987.
- [2] M. Ibsen and R. Feded, "Fiber Bragg gratings for pure dispersion-slope compensation," *Opt. Lett.*, vol. 28, no. 12, pp. 980–982, June 2003.
- [3] S. Kumar and A. Hasegawa, "Quasi-soliton propagation in dispersion-managed optical fibers," *Opt. Lett.*, vol. 22, no. 6, pp. 372–374, Mar. 1997.
- [4] S. K. Turitsyn and V. K. Mezentsev, "Chirped solitons with strong confinement in transmission links with in-line fiber Bragg gratings," *Opt. Lett.*, vol. 23, no. 8, pp. 600–602, Apr. 1998.
- [5] A. B. Grudinin, M. Durkin, M. Ibsen, R. I. Laming, A. Schiffini, P. Franco, E. Grandi, and M. Romagnoli, "Straight line 10Gbit/s soliton transmission over 1000 km of standard fibre with in-line chirped fibre grating for partial dispersion compensation," *Electron. Lett.*, vol. 33, no. 18, pp. 1572–1573, Aug. 1997.
- [6] E. Yamada, T. Imai, T. Komukai, and M. Nakazawa, "10 Gbit/s soliton transmission over 2900 km using 1.3 μ m singlemode fibres and dispersion compensation using chirped fibre Bragg gratings," *Electron. Lett.*, vol. 35, no. 9, pp. 728–729, Apr. 1999.
- [7] P. Li, J. Shuisheng, Y. Fengping, N. Tigan, and W. Zhi, "Long-haul WDM system through conventional single mode optical fiber with dispersion compensation by chirped fiber Bragg grating," *Opt. Commun.*, vol. 222, no. 1–6, pp. 169–178, Jul. 2003.
- [8] A. Sahara, T. Komukai, E. Yamada, and M. Nakazawa, "40 Gbit/s return-to-zero transmission over 500 km of standard fibre using chirped fibre Bragg gratings with small group delay ripples," *Electron. Lett.*, vol. 37, no. 1, pp. 8–9, Jan. 2001.
- [9] T. Komukai, T. Inui, and M. Nakazawa, "Origin of group delay ripple in chirped fiber Bragg gratings and its effective reduction method," *Electron. Commun.*, vol. 86, no. 8, pp. 76–84, Jul. 2003, in Japan, Part 2.
- [10] S. G. Evangelides, N. S. Bergano, and C. R. Davidson, "Intersymbol interference induced by delay ripple in fiber Bragg gratings," in *Proc. Opt. Fiber Commun. Conf.*, Washington, DC, 1999, vol. 4, pp. 5–7, OSA Tech. Dig. Ser. Opt. Soc. Amer. 1999.
- [11] C. Scheerer, C. Glingener, G. Fischer, M. Bohn, and W. Rosenkranz, "System impact of ripples in grating group delay," in *Proc. Int. Conf. Transpar. Opt. Netw. 1999*, 1999, pp. 33–36.
- [12] K. Ennsner, M. Ibsen, M. Durkin, M. N. Zervas, and R. I. Laming, "Influence of nonideal chirped fiber grating characteristics on dispersion cancellation," *IEEE Photon. Technol. Lett.*, vol. 10, no. 10, pp. 1476–1478, Oct. 1998.
- [13] Y. H. C. Kwan, P. K. A. Wai, and H. Y. Tam, "Effect of group-delay ripples on dispersion-managed soliton communication systems with chirped fiber gratings," *Opt. Lett.*, vol. 26, no. 13, pp. 959–961, Jul. 2001.
- [14] J. D. Ania-Castañón, P. García-Fernández, and J. M. Soto-Crespo, "Fiber Bragg grating dispersion-managed multisolitons," *J. Opt. Soc. Amer. B*, vol. 18, no. 9, pp. 1252–1259, Sep. 2001.
- [15] M. Sumetsky, P. I. Reyes, P. S. Westbrook, N. M. Litchinitser, B. J. Eggleton, Y. Li, R. Deshmukh, and C. Socolich, "Group-delay ripple correction in chirped fiber Bragg gratings," *Opt. Lett.*, vol. 28, no. 10, pp. 777–779, May 2003.
- [16] J. T. Mok, J. L. Blows, and B. J. Eggleton, "Investigation of group delay ripple distorted signals transmitted through all-optical 2R regenerators," *Opt. Express*, vol. 12, no. 19, pp. 4411–4422, Sep. 2004.
- [17] N. J. Doran and D. Wood, "Nonlinear-optical loop mirror," *Opt. Lett.*, vol. 13, no. 1, pp. 56–58, Jan. 1988.
- [18] N. J. Smith and N. J. Doran, "Picosecond soliton transmission using concatenated nonlinear optical loop-mirror intensity filters," *J. Opt. Soc. Amer. B*, vol. 12, no. 6, pp. 1117–1125, Jun. 1995.
- [19] S. Boscolo, S. K. Turitsyn, and K. J. Blow, "All-optical passive 2R regeneration for $N \times 40$ Gbit/s WDM transmission using NOLM and novel filtering technique," *Opt. Commun.*, vol. 217, no. 1–6, pp. 227–232, Mar. 2003.
- [20] A. Gray, Z. Huang, Y. W. A. Lee, I. Y. Khrushchev, and I. Bennion, "Experimental observation of autosoliton propagation in a dispersion-managed system guided by nonlinear optical loop mirrors," *Opt. Lett.*, vol. 29, no. 9, pp. 926–928, May 2004.
- [21] S. Boscolo, J. H. B. Nijhof, and S. K. Turitsyn, "Autosoliton transmission in dispersion-managed systems guided by in-line nonlinear optical loop mirrors," *Opt. Lett.*, vol. 25, no. 17, pp. 1240–1242, Sep. 2000.
- [22] F. Seguinéau, B. Lavigne, D. Rouvillain, P. Brindel, L. Pierre, and O. Leclerc, "Experiment demonstration of simple NOLM-based 2R regenerator for 42.66 Gbit/s WDM long-haul transmissions," in *Proc. Opt. Fiber Commun. Conf.*, Washington, DC, 2004, Opt. Soc. Amer. 2004 Paper WN4.
- [23] Y. H. C. Kwan, K. Nakkeeran, P. K. A. Wai, and P. Tchofo Dinda, "Gaussian pulse propagation in dispersion-managed systems using chirped fiber gratings with group delay ripples," *IEEE Photon. Technol. Lett.*, vol. 17, no. 5, pp. 1025–1027, May 2005.
- [24] Y. H. C. Kwan, K. Nakkeeran, and P. K. A. Wai, "Analytical method for designing grating compensated dispersion-managed soliton systems," *J. Opt. Soc. Amer. B*, vol. 21, no. 4, pp. 706–718, Apr. 2004, selected by *Virtual J. Ultrafast Sci.*, 3 issue 4, 2004.
- [25] R. Kashyap, *Fiber Bragg Gratings*. San Diego, CA: Academic, 1999, ch. 4.
- [26] Y. H. C. Kwan, K. Nakkeeran, P. K. A. Wai, and P. Tchofo Dinda, "Significant improvement of performance in grating-compensated transmission systems using nonlinear optical loop mirrors," in *Proc. Int. Conf. Commun. Netw. (ICOCN)*, 2004, pp. 39–42.
- [27] H. Chotard, Y. Painchaud, A. Mailloux, M. Morin, F. Trépanier, and M. Guy, "Group delay ripple of cascaded Bragg grating gain flattening filters," *IEEE Photon. Technol. Lett.*, vol. 14, no. 8, pp. 1130–1132, Aug. 2002.
- [28] Y. H. C. Kwan, K. Nakkeeran, P. K. A. Wai, and P. Tchofo Dinda, "Reduction of intersymbol interference in dispersion managed soliton systems compensated by chirped fibre gratings using nonlinear optical loop mirrors," *J. Opt. A: Pure Appl. Opt.*, vol. 7, pp. 315–323, Jun. 2005.
- [29] K. Nakkeeran, Y. H. C. Kwan, P. K. A. Wai, A. Labruyère, P. Tchofo Dinda, and A. B. Moubissi, "Analytical design of densely dispersion-managed optical fiber transmission systems with Gaussian and raised cosine return-to-zero *Ansätze*," *J. Opt. Soc. Amer. B*, vol. 21, no. 11, pp. 1901–1907, Nov. 2004.
- [30] P. Tchofo Dinda, A. Labruyère, and N. Kakkeeran, "Theory of Raman effect on solitons in optical fibre systems: impact and control processes for high-speed long-distance transmission lines," *Opt. Commun.*, vol. 234, no. 1–6, pp. 137–151, Apr. 2004.



Y. H. C. Kwan (M'05) received the B.S.(Hons.), M.Phil., and Ph.D. degrees from The Hong Kong Polytechnic University, Hong Kong, in 1997, 2001, and 2006, respectively.

She is working as an Engineer in Hong Kong Science and Technology Parks Corporation, Hong Kong, since 2005. Currently, she is also a visitor with The Hong Kong Polytechnic University. Her research interests include optical communications, dispersion management, chirped fiber gratings, and nonlinear optical loop mirrors.

Dr. Kwan has received numerous awards and grants from the IEEE and Optical Society of America (OSA), including the IEEE LEOS Japan Chapter Student Award, the JOSA Publications Award, the IEEE LEOS Student Travel Grant, and Incubic/Milton Chang Travel Grant in CLEO 2005. She is a member of the OSA.

K. Nakkeeran received the B.Eng. degree from the Coimbatore Institute of Technology, Coimbatore, India, in 1993, and the M.Tech. and Ph.D. degrees from Anna University, Chennai, India, in 1995 and 1998, respectively.

In 1999, he joined the Institute of Mathematical Sciences, Chennai, where he worked as a Postdoctoral Fellow for 10 months. In 1999, he became a

Research Associate with the Department of Physics, University of Burgundy, Dijon, France. In 2002, he became a Postdoctoral Fellow with the Department of Electronic and Information Engineering, The Hong Kong Polytechnic University. Since 2005, he has been a lecturer with the School of Engineering, University of Aberdeen, U.K. His research interests include solitons, fiber lasers, modeling and simulations of optical devices, long-haul optical fiber communications, and nonlinear science.

Dr. Nakkeeran is a member of the Optical Society of America and IET.



P. K. A. Wai (SM'96) received the B.S. (Hons) degree from the University of Hong Kong in 1981, and the M.S. and Ph.D. degrees from the University of Maryland, College Park, in 1985 and 1988, respectively.

In 1988, he joined Science Applications International Corporation, McLean, VA, where he worked as a Research Scientist on the Tethered Satellite System project. In 1990, he became a Research Associate with the Department of Physics, University of Maryland, and the Department of Electrical Engineering, University of Maryland, Baltimore County. In 1996, he joined

the Department of Electronic and Information Engineering, The Hong Kong Polytechnic University. He became Chair Professor of Optical Communications in 2005. Currently, he is the Dean of the Faculty of Engineering. His research interests include solitons, fiber lasers, modeling and simulations of optical devices, long-haul optical fiber communications, all-optical packet switching, and network theories. He is an active contributor to the field of photonics and optical communications, having more than 250 international refereed publications.

Prof. Wai serves as the Guest Editor of the IEEE JOURNAL ON SELECTED AREAS OF QUANTUM ELECTRONICS and is an editor of *Optics Express*. He is a member of the Optical Society of America.

Patrice Tchofo Dinda received the Ph.D. degree in physics from the University of Dijon, France, in 1991.

In 1992, he carried out a Postdoctoral research study on the melting behavior of silicone clusters at the University of Heraklion, Greece. In 1993, he was an Assistant Professor at the University of Dijon, and since 2002, he has been Professor with the Physics Department at the same university. His current research interests are in the physics of nonlinear effects in optical fibers, modulational instabilities, and dispersion-managed solitons.